Heliyon 9 (2023) e12946

Contents lists available at ScienceDirect

Heliyon

journal homepage: www.cell.com/heliyon

Research article

Effects of sintering condition on giant dielectric and nonlinear current-voltage properties of $Na_{1/2}Y_{1/2}Cu_3Ti_{3.975}Ta_{0.025}O_{12}$ ceramics

Pariwat Saengvong [a], Jakkree Boonlakhorn [b], Jutapol Jumpatam [c], Narong Chanlek [d], Jariyanee Prasongkit [e], Bundit Putasaeng [f], Pairot Moontragoon [a], Pornjuk Srepusharawoot [a,*], Prasit Thongbai [a]

[a] Giant Dielectric and Computational Design Research Group (GD–CDR), Department of Physics, Faculty of Science, Khon Kaen University, Khon Kaen, 40002, Thailand
[b] Department of Basic Science and Mathematics, Faculty of Science, Thaksin University, Songkhla Campus, Songkhla, 90000, Thailand
[c] Department of Fundamental Science, Faculty of Science and Technology, Surindra Rajabhat University, Surin, 32000, Thailand
[d] Synchrotron Light Research Institute (Public Organization), 111 University Avenue, Muang District, Nakhon Ratchasima, 30000, Thailand
[e] Division of Physics, Faculty of Science, Nakhon Phanom University, Nakhon Phanom, 48000, Thailand
[f] National Metal and Materials Technology Center, National Science and Technology Development Agency, Thailand Science Park, Pathum Thani, 12120, Thailand

ARTICLE INFO

Keywords:
Giant dielectric properties
First principle calculations
Microstructure
Maxwell–Wagner polarization
NYCTO

ABSTRACT

The effects of sintering conditions on the microstructure, giant dielectric response, and electrical properties of $Na_{1/2}Y_{1/2}Cu_3Ti_{3.975}Ta_{0.025}O_{12}$ (NYCTTaO) were studied. A single phase of $Na_{1/2}Y_{1/2}Cu_3Ti_4O_{12}$ and a high density (>98.5%) were obtained in the sintered NYCTTaO ceramics. First–principles calculations were used to study the structure of the NYCTTaO. Insulating grain boundaries (i–GBs) and semiconducting grains (semi–Gs) were studied at different temperatures using impedance and admittance spectroscopies. The conduction activation energies of the semi–Gs and i–GBs were $E_g \approx 0.1$ and $E_{gb} \approx 0.6$ eV, respectively. A large dielectric constant ($\varepsilon' \approx 2.43–3.89 \times 10^4$) and low loss tangent ($\tan\delta \approx 0.046–0.021$) were achieved. When the sintering temperature was increased from 1070 to 1090 °C, the mean grain size slightly increased, while ε' showed the opposite tendency. Furthermore, the breakdown electric field (E_b) increases significantly. As the sintering time increased from 5 to 10 h, the mean grain size did not change, whereas ε' and E_b increased. Variations in the dielectric response and non–linear electrical properties were primarily described by the intrinsic (E_{gb}) and extrinsic (segregation of Na–, Cu–, Ta–, and O–rich phases) properties of the i–GBs based on the internal barrier layer capacitor effect.

1. Introduction

Recently, electronic devices driven by advanced materials have been rapidly developed. Electronic devices consist of integrated circuits (ICs) and passive components. For passive components, capacitors are one of the most important components in many

* Corresponding author.
E-mail address: spornj@kku.ac.th (P. Srepusharawoot).

https://doi.org/10.1016/j.heliyon.2023.e12946
Received 3 December 2022; Received in revised form 10 January 2023; Accepted 10 January 2023
Available online 14 January 2023

electronic circuits [1-3]. Developing a dielectric material to increase its performance is essential for improving capacitor technologies that tend to reduce the capacitor size without affecting its capacitance. This can be accomplished by increasing the dielectric constant (ε') of the dielectric layer. Although many parameters of a dielectric material must be considered before considering their use, the fundamental requirements of dielectric materials for capacitor applications are high ε', low loss tangent (tanδ), and excellent temperature and frequency stability [1].

$CaCu_3Ti_4O_{12}$ (CCTO) and related compounds are non–ferroelectric ceramics that can exhibit very large ε' values of 10^3–10^5, depending on the sintering conditions, preparation methods, electrode materials, doping ions, and other parameters [4–10]. A large ε' value was observed over wide temperature and frequency ranges. However, a large tanδ value (>0.05) remains a significant barrier for its application in electronic devices. Thus, the dielectric properties of CCTO ceramics have continuously been improved. The origins of the dielectric and electrical properties of CCTO ceramics have also been intensively studied [4,5,11–17]. The heterogeneous microstructure of CCTO ceramics consists of insulating grain boundaries (i–GBs) and semiconducting grains (semi–Gs). This special microstructure is are referred to as the internal barrier capacitor (IBCL) structure [11,18,19]. The IBLC model is extensively accepted to explain the giant ε' in CCTO–based ceramics. Accordingly, the electrical properties of semi–Gs and i–GBs are important for their dielectric properties and applications. Therefore, investigations of the microstructural evolution, relevant dielectric response, and electrical properties have been widely performed.

Dopant substitution has been used extensively to improve the dielectric and electrical properties of polycrystalline ceramics. For CCTO ceramics, substitution of Ta^{5+} ions caused degradation of the dielectric properties due to a remarkable increase in tanδ, which is undesirable for capacitor applications [15,16,20–23]. The average grain size of Ta^{5+}–doped CCTO decreased with increasing Ti^{5+} content, whereas tanδ was greatly increased because of the destruction of the potential barrier height at the i–GBs. Accordingly, the nonlinear current density–electric field (J–E) properties were also degraded.

Sintering conditions are generally designed and investigated to obtain the designed ceramic microstructure that leads to improved dielectric properties. The microstructure of CCTO–based ceramics can be modified by varying their sintering conditions. The average grain size of CCTO tends to increase with increasing temperature and sintering duration [12,24–27]. Accordingly, the ε' value of undoped CCTO increased continuously with sintering time and temperature. Furthermore, the sintering conditions can control the nonlinear J–E properties of CCTO ceramics [7,24,25].

In addition to CCTO, other oxides in the $ACu_3Ti_4O_{12}$ family (A = $Na_{1/2}Y_{1/2}$, $Na_{1/2}B_{1/2}$, $Y_{3/2}$, $B_{3/2}$, Cd, $La_{2/3}$, $Sm_{2/3}$, $Na_{1/2}Sm_{1/2}$, and others) have also been systematically studied because of their large ε' values with relatively low tanδ compared to that of CCTO [9,10,17,28–34]. Among them, the $Na_{1/2}Y_{1/2}Cu_3Ti_4O_{12}$ (NYCTO) ceramic has received extensive attention because it exhibited a high $\varepsilon'>10^4$ and low tanδ<0.1 [12,35–37]. Most recently, we found that the substitution of NYCTO ceramics with Ta^{5+} on the Ti^{4+} (NYCTTaO) site can improve the dielectric properties [38]. Furthermore, computational calculations of the NYCTTaO structure have not yet been reported. Thus, the NYCTTaO ceramic is one of the most interesting oxides in the $ACu_3Ti_4O_{12}$ family. Unfortunately, the effects of sintering conditions on the microstructure and dielectric properties, as well as the nonlinear J–E properties, have not been reported. The investigation of sintering effects may provide important results to clearly understand the dielectric response behavior of NYCTO ceramics.

In this study, we synthesized $Na_{1/2}Y_{1/2}Cu_3Ti_{3.975}Ta_{0.025}O_{12}$ ceramics using the solid–state reaction (SSR) method under different temperature conditions. First–principles calculations were used to study the structure of the NYCTTaO. The effect of sintering on the microstructure of the ceramics was also investigated. The dielectric properties were analyzed as functions of frequency and temperature. The electrical behavior was studied using impedance and admittance spectroscopies. The origins of the dielectric and nonlinear electrical properties were discussed in detail.

2. Experimental methods

2.1. Experimental details

The $Na_{1/2}Y_{1/2}Cu_3Ti_{3.975}Ta_{0.025}O_{12}$ powder was prepared using SSR method. Na_2CO_3 (99.9%), Y_2O_3 (99.99%), CuO (99.9%), Ta_2O_5 (99.99%), and TiO_2 (99.9%) were mixed using a wet ball–milling method in ethanol for 24 h; the details are explained in a previous work [8]. The ceramic samples were obtained by sintering the compact powders at 1070 °C for 5 and 10 h and sintering at 1080 and 1090 °C for 5 h. These samples are referred to as the 1NYCTTaO, 2NYCTTaO, 3NYCTTaO, and 4NYCTTaO samples, respectively.

The phase compositions were measured by X–ray diffraction (XRD, PANalytical, EMPYREAN). The XRD results were analyzed using Rietveld refinement. The densities of the ceramics were measured using Archimedes' method. The surface microstructure was analyzed using a scanning electron microscope (SEM, MiniSEM, SEC, SNE–4500 M). The elemental components were analyzed by SEM mapping using field-emission scanning electron microscopy. The samples were characterized by the X–ray photoemission spectroscopy (XPS, PHI5000 VersaProbe II, ULVAC–PHI). The details of the dielectric and electrical measurements are described in our previous study [21]. The dielectric properties were measured in the frequency range of 10^2–10^6 Hz and the temperature range of −60 °C–210 °C. The nonlinear J–E properties were tested at 25 °C.

2.2. Computational details

The most preferable locations for Ta and oxygen vacancies in NYCTO were computed using the Vienna *Ab initio* Simulation Package (VASP) [39] which is a software based on density functional theory. The Perdew–Burke–Ernzerhof [40] exchange correlation functional was chosen under the PAW pseudopotential. The valence states of Cu, Ti, and O were reported in a previous work [8]. For Y, 4*s*,

4*p*, 5*s*, and 4*d* valence states were used. Additionally, we used the 2*s*, 2*p*, and 3*s* states and the 5*p*, 5*d*, and 6*s* states for Na and Ta, respectively. For all calculations, a plane–wave energy cut–off of 470 eV was used. Furthermore, the- Γ–point of *k*–point mesh was chosen because of the very large size of the used structure.

3. Results and discussion

The phase formation of the NYCTTaO ceramics that were sintered under various conditions was confirmed by XRD patterns, as shown in Fig. 1. All samples show a single phase of NYCTO without a detectable second phase. The lattice parameters (*a*) of the 1NYCTTaO, 2NYCTTaO, 3NYCTTaO, and 4NYCTTaO ceramics were calculated using the Rietveld refinement method and found to be 7.386, 7.386, 7.387, and 7.387 Å, respectively. These values are comparable to those reported in the literature [21,35–37,41]. The *a* values did not significantly change with sintering time and temperature.

According to the XRD patterns, obviously, the crystal structure of NYCTTaO is identical to that of the CCTO lattice. Therefore, the CCTO lattice was used as the initial structure in the calculations. To determine the stable structure of NYCTTaO, we must determine the locations of the Na and Y dopants in the CCTO lattice. Various experimental results reported in the literature for Y–doped CCTO [42,43] disclosed that the lattice constant of this structure is reduced because the larger ionic radius of the host ions (Ca) is replaced by the doping ions with smaller ionic radius. The ionic radii of Y^{3+} with 9 coordination numbers, Cu^{2+} with 6 coordination numbers, and Ca^{2+} with 12 coordination numbers are 1.07, 0.73 and 1.34 Å, respectively [44]. The ionic radius of Y^{3+} is smaller than that of Ca^{2+} but larger than that of Cu^{2+}. Hence, in this case, the Y^{3+} ions preferentially occupy the Ca sites. Next, the most favorable sites for Na^{+} doping ions were considered. For $Na_{1/2}Sm_{1/2}Cu_3Ti_4O_{12}$ [45], Na is likely to occupy Cu sites. Therefore, in the current study, Na and Y ions occupy the Cu and Ca sites, respectively. In this study, a 5 × 2 × 2 supercell of the NYCTO structure was used as the initial structure. This structure has 800 atoms in total: 40 atoms of Na, 40 atoms of Y, 80 atoms of Cu, 160 atoms of Ti, and 480 atoms of O. The oxidation state of Ta is 5+. Consequently, Ta^{5+} can only occupy Ti^{4+} sites in the NYCTO structure. The substitution of Ta^{5+} at the Ti^{4+} sites resulted in the reduction of Ti^{4+} to Ti^{3+}. For the NYCTTaO structure, one Ta atom was substituted at the Ti site in the supercell. Its chemical formula is $Na_{40}Y_{40}Cu_{80}Ti_{159}TaO_{480}$ and its crystal structure is presented in Fig. 2.

Oxygen vacancies (V_o) are usually occurred during the sintering process, leading to determine the stable position of V_o in the NYCTTaO lattice (Fig. 2). In our calculations, two possible positions of V_o were considered, as presented in Fig. 3(a and b). Fig. 3 (a) shows that V_o was located close to the Ta atom. In contrast, V_o was far from the Ta atom, as shown in Fig. 3 (b). The total energies corresponding to these two structures are shown in Fig. 3 (c). The total energy of Structure B was lower than that of Structure A at 0.583 eV. Hence, based on this result, Ta could not induce V_o in the NYCTTaO structure.

Next, we calculated the different electron densities between the NYTTO structures with and without V_o ($\Delta D(r)$), as shown by the following relation: $\Delta D(r) = \rho_{NYCTTO+Vo}(r) - \rho_{NYCTTO}(r)$, where $\rho_{NYCTTO+Vo}(r)$ is the electron density of structure A in Fig. 3 (a). In addition, $\rho_{NYCTTO}(r)$ represents the electron density of the NYCTTaO structure, as shown in Fig. 2. The calculated positive $\Delta D(r)$ results are shown in Fig. 4. Positive $\Delta D(r)$ refers to $\rho_{NYCTTO+Vo}(r) > \rho_{NYCTTO}(r)$. This is directly related to the electron accumulation in NYCTTaO in the presence of V_o, resulting in the reduction of the oxidation states of cations. The oxidation states of Cu and Ti in this structure are 2+ and 4+, respectively. As shown in Fig. 4, there were pink shades for both Cu and Ti ions. Therefore, the oxidation state of these ions decreased. Consequently, the charge states of Cu and Ti can be reduced from Cu^{2+} to Cu^{+} and Ti^{4+} to Ti^{3+}, respectively. By considering the $\Delta D(r)$ of the Ta ion, it was found that the $\Delta D(r)$ is unchanged. This result indicates that the oxidation state of Ta is unaltered when V_o is present in the NYCTTaO structure. Based on our electron density analysis, the charges of Cu and Ti tend to be reduced, whereas the oxidation state of Ta remains unchanged when V_o is present in the NYCTTaO lattice. This was also observed for the $Na_{1/2}Sm_{1/2}Cu_3Ti_4O_{12}$ [45] and $Na_{1/3}Sm_{1/3}Ca_{1/3}Cu_3Ti_4O_{12}$ [46].

Fig. 5(a–d) show the SEM images of the polished surface morphologies of the 1NYCTTaO, 2NYCTTaO, 3NYCTTaO, and 4NYCTTaO ceramics, respectively. A small number of pores are observed. Additionally, the grain size distributions of these samples are presented

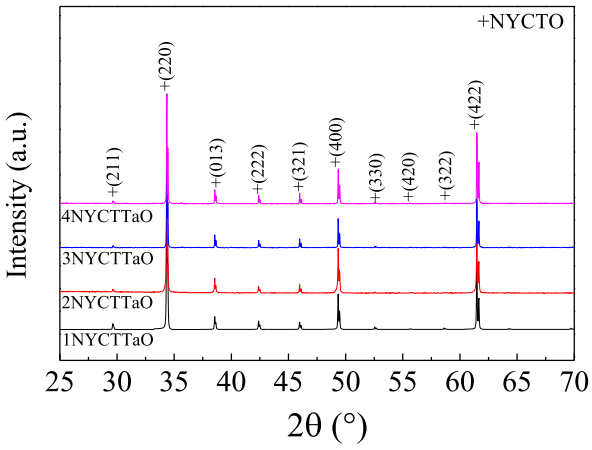

Fig. 1. XRD patterns of $Na_{1/2}Y_{1/2}Cu_3Ti_{3.975}Ta_{0.025}O_{12}$ with different sintering durations and temperatures.

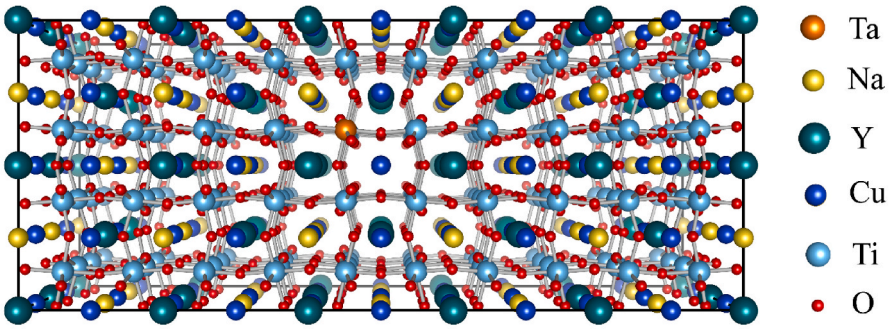

Fig. 2. Crystal structure of NYCTTaO. The orange, yellow, green, dark blue, sky blue, and red balls represent Ta, Na, Y, Cu, Ti, and O, respectively. The bold line indicates the supercell of the structure. (For interpretation of the references to colour in this figure legend, the reader is referred to the Web version of this article.)

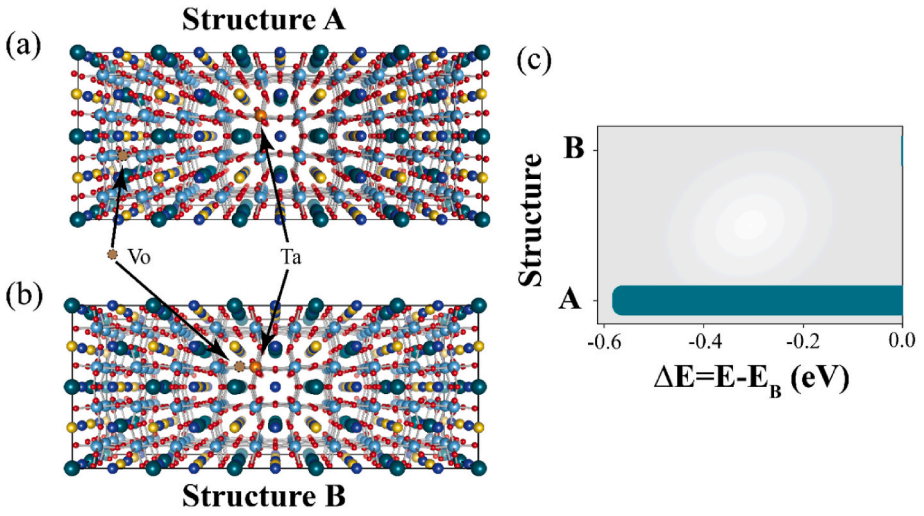

Fig. 3. (a) Ta was independent of Ta atoms. (b) Ta atom is in close proximity to Vo. (c) Total energy associated with structures A and B.

in Fig. 5(e–h). It was found that the mean grain sizes (G) were calculated and found to be 20.67 ± 11.39, 20.56 ± 8.69, 29.25 ± 16.68, and 32.79 ± 14.65 mm, respectively. G did not change as the sintering duration increased from 5 to 10 h (sintered at 1070 °C). When the sintering temperature increased from 1070 to 1090 °C for 5 h, G tended to increase. Grain growth is likely associated with the liquid–phase sintering mechanism because the eutectic temperatures of CuO–TiO_2 are ≈919 °C [35,37,47]. The grain growth in polycrystalline ceramics is primarily driven by atom and ion diffusion, which usually increase with increasing sintering temperature. The relative densities of the 1NYCTTaO, 2NYCTTaO, 3NYCTTaO, and 4NYCTTaO ceramics are 98.75, 99.68, 99.20, and 99.10%, respectively.

The EDS was performed to further characterize the microstructure. The EDS spectrum of the 2NYCTTaO ceramic is shown in Fig. 6 (a), confirming the presence of all elements in the sample (i.e., Na, Y, Ti, O, and Ta). The distribution of all elements in the microstructure was investigated using SEM mapping. As shown in Fig. 6 (b), all elements were homogeneously dispersed inside the grains. However, the accumulation of Ta, Na, Cu, and O segregated along the GBs. The segregation of Ta_2O_5 at the GBs is usually observed in Ta–doped TiO_2, while the segregation of CuO and/or Cu_2O is occasionally observed in CCTO–based ceramics [13,21,35,37,48,49]. Segregation of the Na–rich phase may be associated with a low melting point of Na_2CO_3. Precipitation of the Na–liquid phase along the GBs may have occurred during the cooling stage.

The dielectric response of the NYCTTaO ceramics sintered under various sintering conditions in the frequency range of 10^2–10^6 Hz (at 20 °C) is shown in Fig. 7 (a). The ε′ values at 1 kHz for the 1NYCTTaO, 2NYCTTaO, 3NYCTTaO, and 4NYCTTaO ceramics are 35,962, 38,949, 28,004, and 24,321, respectively. The ε′ value increased with increasing sintering duration, which is similar to that reported for NYCTO ceramics [37]. However, the dielectric response declined as the sintering temperature increased, even though the mean grain size increased. As shown in Fig. 7 (b), the tanδ values of 1NYCTTaO, 2NYCTTaO, 3NYCTTaO, and 4NYCTTaO at 1 kHz are 0.046, 0.026, 0.021, and 0.029, respectively. Furthermore, the tanδ values of the 2NYCTTaO, 3NYCTTaO, and 4NYCTTaO ceramics are lower than 0.09 over the frequency range of 10^2–10^5 Hz. A high–frequency tanδ rapidly increases with increasing frequency, which is a

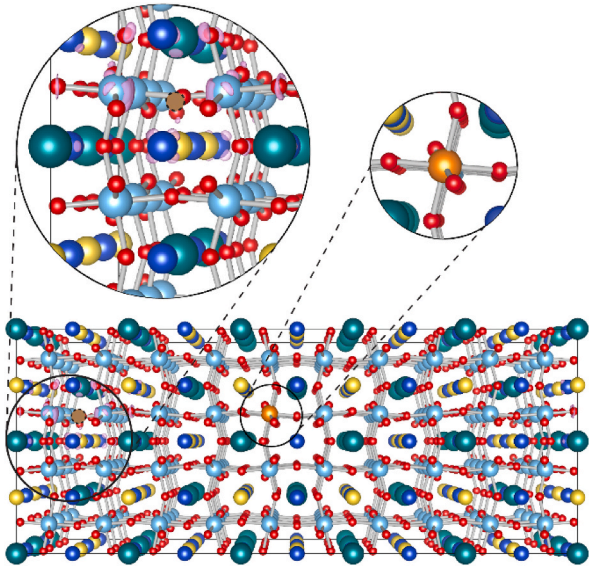

Fig. 4. Positive $\Delta D(r)$ is represented by the pink regions. Ta, Na, Y, Cu, Ti, and O are denoted by orange, yellow, green, dark blue, sky blue, and red spheres, respectively. (For interpretation of the references to colour in this figure legend, the reader is referred to the Web version of this article.)

partial part of the tanδ relaxation peak. This observation is attributed to the dielectric relaxation mechanism [20]. In a low–frequency range, tanδ increases as the frequency decreased. This result is usually associated with the DC conduction of free charge carriers. According to these results, the dielectric properties of the NYCTTaO ceramics changed with the sintering conditions. The variations in dielectric properties with temperature were also studied, as shown in Fig. 7 (c), where the temperature stability of ε' is quite good from −60 to 150 °C. tanδ strongly increased at high temperatures, which was attributed to the effect of the long–range motion of free charges. This observation is usually observed in both NYCTO and CCTO ceramics [14,47,50–52].

To explain the dielectric response mechanism of the NYCTTaO ceramics sintered under different conditions, the electrical properties of the semi–Gs and i–GBs were characterized using an impedance spectroscopy (IS) [5,16]. Normally, the dielectric and electrical properties of semi–Gs and i–GBs are closely related [12,36,37]. By using Eq. (1), the resistances of semi–Gs (R_g) and i–GBs (R_{gb}) can be calculated from the complex impedance plane (Z*) plot, using the following equation:

$$Z^* = Z' - iZ'' = \frac{1}{j\omega c_0 \varepsilon^*} + \frac{1}{j\omega c_0 (\varepsilon' - i\varepsilon'')} \tag{1}$$

where $Z^* = Z' - iZ''$ is the complex impedance, $\omega = 2\pi f$ is angular frequency (rad/s), $C_0 = \varepsilon_0 A/d$ is the capacitance of free space (F), and $\varepsilon^* = \varepsilon' - i\varepsilon''$ is the complex dielectric permittivity.

Fig. 8 (a) shows the Z* plots of the NYCTTaO ceramics. According to the IBLC model, R_{gb} can be calculated from the diameter of a large semicircular arc of Z* plot [5,24]. At 20 °C, only part of the large arc can be observed. Nevertheless, it can be estimated that the R_{gb} value of the 1NYCTTaO ceramic is the lowest. As shown in the inset of Fig. 8 (a), a nonzero intercept on the Z′−axis can be observed, indicating the existence of semi–Gs [11]. Therefore, the NYCTTaO ceramics are electrically heterogeneous, consisting of semi–Gs and i–Gs. The R_g value of the 1NYCTTaO ceramic was the largest. When the sintering temperature and duration increased, the V_o concentration likely increased because of oxygen loss during the sintering process. Accordingly, the number of free electrons inside the semi–Gs increased, resulting in an increased conductivity inside the semi–Gs or decreased R_g value. When the measured temperature increased, a large arc can be observed, as shown in Fig. 8 (b). The diameter of the large arc shortens with increasing temperature. Accordingly, the R_{gb} values at different temperatures can be calculated. Similarly, the R_g values also changed with temperature. To obtain the calculated R_g and R_{gb} values, Z* plots were fitted using the following equation [4,47]:

$$Z^* = R_g + \frac{R_{gb}}{1 + (i\omega R_{gb} C_{gb})^{\alpha}} \tag{2}$$

where C_{gb} (F) is the capacitance of the i–GBs and α is a constant value ($0 < \alpha \leq 1$). Fig. 8 (b) shows the fitting results obtained using Eq. (2) for the 3NYCTTaO ceramic in the temperature range of 150–210 °C. Accordingly, R_{gb} values at different temperatures were obtained. The Z* plots of the other samples were also well fitted using Eq. (2). As shown in Fig. 8 (c), the temperature dependence of R_{gb} follows the Arrhenius equation [16]:

$$R_{gb} = R_0 \exp\left(\frac{E_{gb}}{k_B T}\right) \tag{3}$$

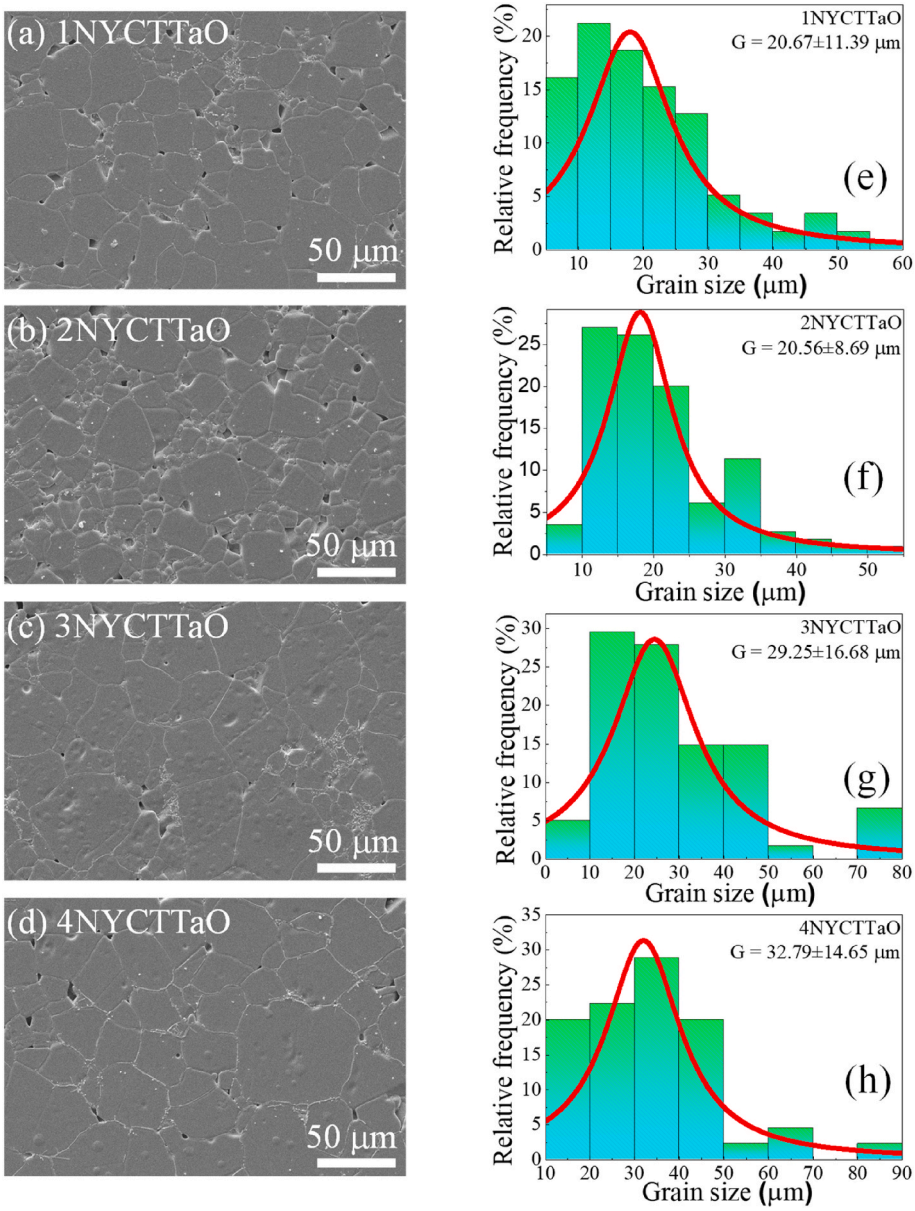

Fig. 5. (a–d) SEM images of polished surfaces and (e–h) grain size distributions of 1NYCTTaO, 2NYCTTaO, 3NYCTTaO, and 4NYCTTaO samples.

where k_B and R_0 are the Boltzmann constant (J/K) and the exponential term, respectively. The activation energies (E_{gb}) can be calculated by using Eq. (3) and found to be 0.566, 0.635, 0.605, and 0.652 eV for the 1NYCTTaO, 2NYCTTaO, 3NYCTTaO, and 4NYCTTaO ceramics, respectively. These values were closed to that reported in the NYCTO ceramics [35,37,47]. This finding confirms the electrical insulation characteristics of the i–GBs. Moreover, the E_{gb} values tend to increase with increasing sintering duration, which may primarily be due to the segregation of metal oxide–rich phases along the i–GBs, as shown in Fig. 6 (b). Likewise, increasing the sintering temperature also resulted in an increase in E_{gb} with the same cause. The reduction in the tanδ values of the NYCTTaO ceramics may be caused by the enhanced R_{gb} and E_{gb}, following the IBLC model [12,37,53]. Therefore, the electrical properties of i–GBs and the correlated dielectric properties of the NYCTTaO ceramics were dependent on the sintering conditions.

Based on the IBLC model, the electrical properties of the semi–Gs are also important, affecting the dielectric properties. Generally, the electrical response of the semi–Gs is analyzed from the non–zero intercept on the Z′–axis of the Z* plot when a small semicircular arc cannot be observed in the measured temperature and frequency ranges. An alternative method that can be applied to characterize the semi–G response is admittance spectroscopy, using the complex admittance (Y*), as expressed by the following equation:

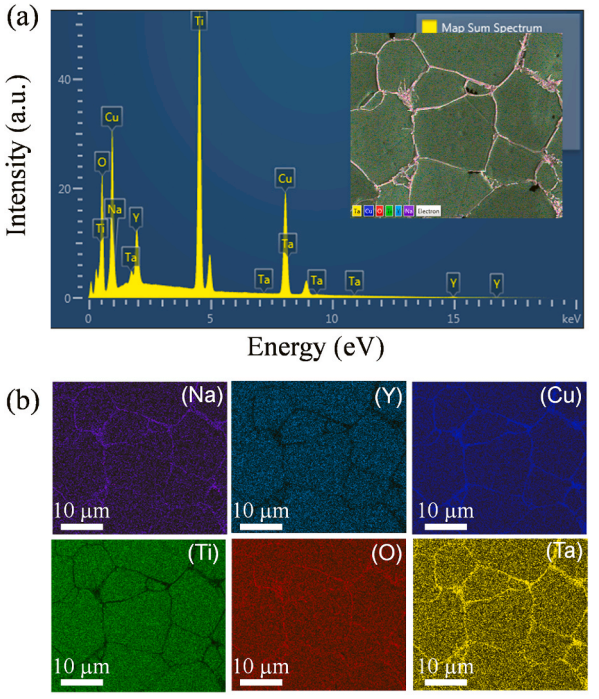

Fig. 6. (a) EDS spectrum of 2NYCTTaO; inset shows the selected area for the measurement of EDS mapping images. (b) SEM elemental mapping images of Na, Y, Cu, Ti, O, and Ta.

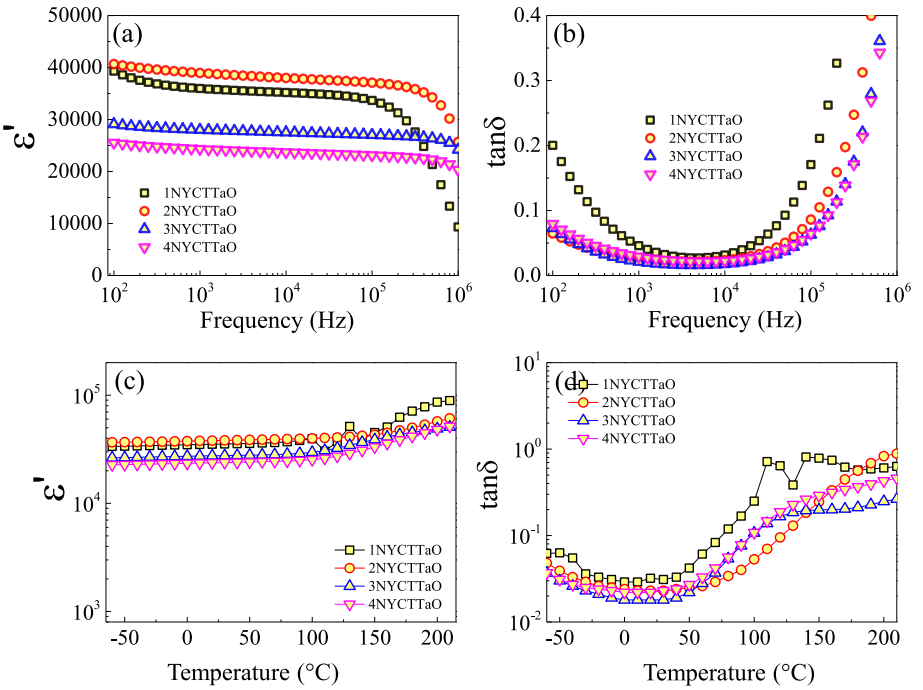

Fig. 7. (a–b) ε′ and tanδ at 20 °C as a function of the frequency for $Na_{1/2}Y_{1/2}Cu_3Ti_{3.975}Ta_{0.025}O_{12}$ under different sintering conditions. (c–d) Temperature dependences of ε′ and tanδ at 10 kHz.

$$Y^* = \frac{\left(R_{gb}^{-1}\right)\left(1 - \omega^2\tau_g\tau_{gb} + i\omega\tau_{gb}\right)}{1 + i\omega\tau} \tag{4}$$

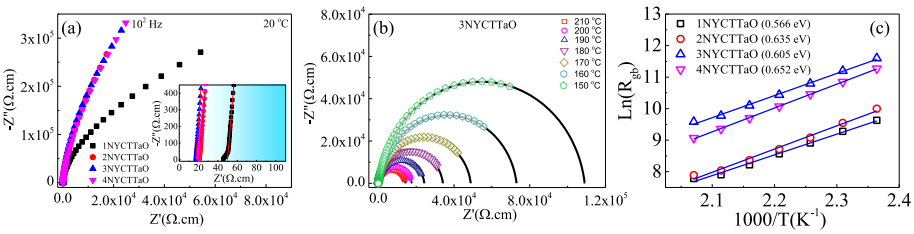

Fig. 8. (a) Z* plots at 20 °C for $Na_{1/2}Y_{1/2}Cu_3Ti_{3.975}Ta_{0.025}O_{12}$ under different sintering conditions; inset displays a non–zero intercept on the Z′ axis. (b) Fitting curves of Z* at different temperatures for the 3NYCTTaO sample. (c) Arrhenius plots of R_{gb}.

where $\tau = R_gC_{gb}$ (s), $\tau_g = R_gC_g$, and $\tau_{gb} = R_{gb}C_{gb}$. Form (Eq. (4)), R_g can be calculated from the relationship $R_g = 1/2Y''_{max}$ (Y''_{max} is the maximum value at Y'' peak). Fig. 9(a–d) show the frequency dependence of Y'' of the 3NYCTTaO and 4NYCTTaO ceramics in the temperature range from −60 to 0 °C. The activation energy required for charge transfer inside the semi–Gs (E_g) can be calculated using the Arrhenius equation of the conductivity ($\sigma_g \propto 1/R_g$):

$$\sigma_g = \sigma_0 e^{\left(\frac{-E_g}{k_B T}\right)} \tag{5}$$

The temperature dependence of the σ_g can be linearly fitted using Eq. (5), as shown in the insets of Fig. 9(a–d). The calculated E_g values of the 1NYCTTaO, 2NYCTTaO, 3NYCTTaO, and 4NYCTTaO ceramics are 0.119, 0.110, 0.107, and 0.108 eV, respectively. All E_g values are similar to those reported for NYCTO and CCTO ceramics [35,37,54,55], confirming the semi–Gs of NYCTTaO. Note that the E_g values tended to slightly decrease with increasing the sintering temperature and time. These results might be associated with oxygen loss from the lattice during the sintering process, resulting in a slight increase in free electrons.

Fig. 10(a and b) show the XPS spectra for Cu2 $p_{3/2}$ of the 1NYCTTaO and 2NYCTTaO ceramics, respectively. The XPS spectra were fitted using Gaussian–Lorentzian fitting. The binding energies of the Cu^{1+}, Cu^{2+}, and Cu^{3+} peaks were 932.62, 934.36, and 936.00 eV, respectively. Different oxidation states of Cu, i.e., Cu^{1+}, Cu^{2+}, and Cu^{3+}, were detected. The calculated ratios of Cu^{+}/Cu^{2+} and Cu^{3+}/Cu^{2+} in the 1NYCTTaO (43.79% and 20.65%, respectively) and 2NYCTTaO ceramics (44.05% and 33.57%) were obtained. The ratios tended to increase with increasing sintering time, corresponding to the reduced E_g. A small Ti^{3+}/Ti^{4+} ratio was detected in the XPS spectra, as shown in Fig. 10(c and d). Thus, semi–Gs originate from charge hopping between $Cu^{+} \leftrightarrow Cu^{2+}$, $Cu^{2+} \leftrightarrow Cu^{3+}$, and $Ti^{3+} \leftrightarrow Ti^{4+}$, depending on the charge carrier concentration [15,20,56]. An increased carrier concentration resulted in the increase in the conductivity of semi–Gs.

The effect of sintering conditions on the electrical properties of the i–GBs was investigated via the J–E characteristics, as shown in Fig. 11. The breakdown electric fields (E_b) of the 1NYCTTaO, 2NYCTTaO, 3NYCTTaO, and 4NYCTTaO ceramics occurred at 123.1, 300.6, 373.4, and 653.9 eV, respectively. The nonlinear coefficient (α) values were 3.9, 5.9, 4.6, and 5.0, respectively. The E_b values increased with increasing sintering duration and temperature. Generally, non–linear J–E behaviors are caused by Schottky barriers at i–GBs, which are created in the heterogeneous microstructure of many ceramic oxides [5,6,57,58]. Thus, the non–linear J–E properties are associated with both the intrinsic (potential barrier height, Φ_b) and extrinsic (microstructure) factors of the i–GBs. For the intrinsic factor, the increased E_b value was attributed to the enhanced Φ_b, which was reflected in the increased E_{gb}. Moreover, the increased E_b values were also related to the microstructure with segregation of metal oxide–rich phases along the i–GBs even though the mean grain size slightly increased. The non–linear properties of NYCTTaO ceramics are related to the E_{gb} and R_{gb} values. The overall results indicate that the sintering duration and temperature influence the dielectric and electrical properties of the NYCTTaO ceramics.

4. Conclusion

Single phase NYCTTaO ceramics were successfully synthesized using the SSR method and sintered under various conditions. Segregation of Na–, Cu–, Ta–, and O–rich phases was observed along the i–GBs. The electrical properties of the i–GBs with $E_{gb} \approx 0.6$ eV and semi–Gs ($E_g \approx 0.1$ eV) were investigated using impedance spectroscopy. The sintered NYCTTaO ceramics exhibited high ε′ values of 2.43–3.89 × 10^4 and low tanδ ≈0.046–0.021. The oxidation states of Cu^{1+}, Cu^{2+}, Cu^{3+}, Ti^{3+}, and Ti^{4+}, which are the origins of the semi–Gs, were detected. When the sintering temperature was increased from 1070 to 1090 °C, ε′ decreased, whereas the mean grain size slightly increased. Nevertheless, E_b increased significantly owing to the increased E_{gb} and segregation of metal oxides along the i–GBs. When the sintering time was increased from 5 h to 10 h, the ε′ and E_b were enhanced, which were not related to the mean grain size. The dielectric and non–linear electrical properties were reasonably explained using the IBLC model and associated with the intrinsic and extrinsic properties of the i–GBs.

Author contribution statement

Pariwat Saengvong: Performed the experiments.

Jakkree Boonlakhorn, Jutapol Jumpatam, Narong Chanlek, Jariyanee Prasongkit, Bundit Putasaeng, Pairot Moontragoon: Analyzed and interpreted the data.

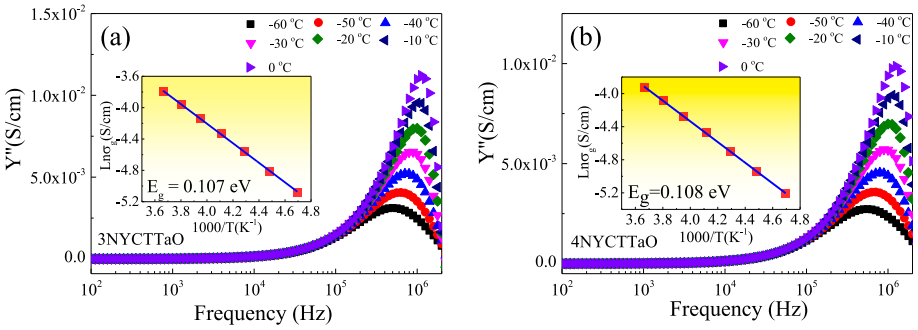

Fig. 9. Frequency dependence of Y″ of (a) 3NYCTTaO and (b) 4NYCTTaO; their insets show Arrhenius plots of σ_g.

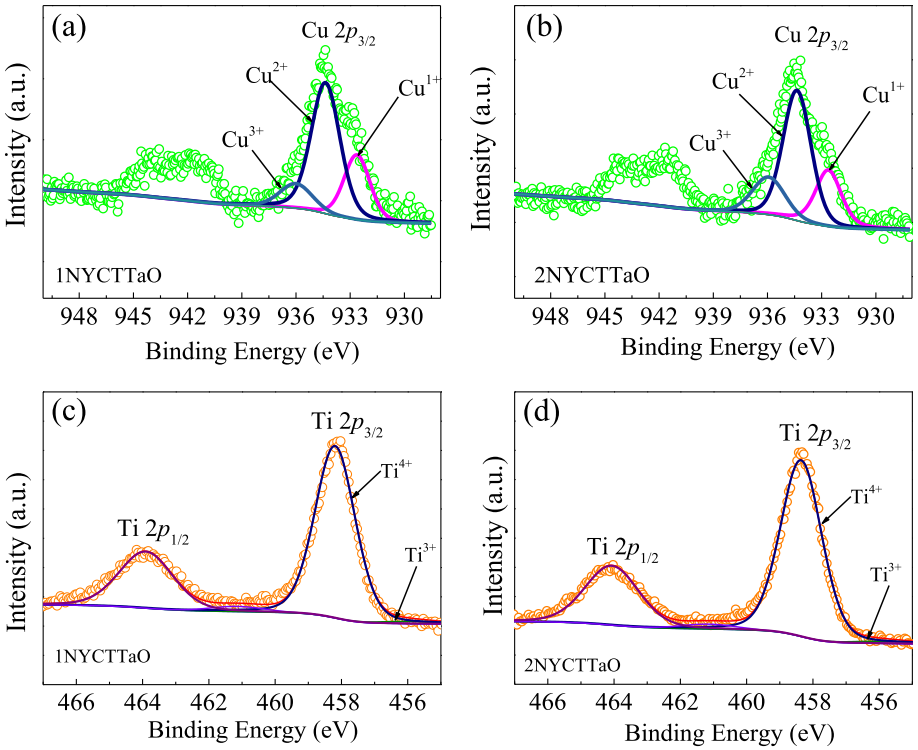

Fig. 10. XPS spectra of (a–b) Cu and (c–d) Ti in the 1NYCTTaO and 2NYCTTaO samples.

Pornjuk Srepusharawoot, Prasit Thongbai: Conceived and designed the experiments; Contributed reagents, materials, analysis tools or data; Wrote the paper.

Funding statement

This work was supported by The Program Management Unit for Human Resources & Institutional Development, Research and Innovation (Grant No.B05F650017) and Research and Graduate Studies of Khon Kaen University. P. Saengvong would like to thank the Science Achievement Scholarship of Thailand for his scholarship.

Data availability statement

Data will be made available on request.

Declaration of interest's statement

The authors declare no competing interests.

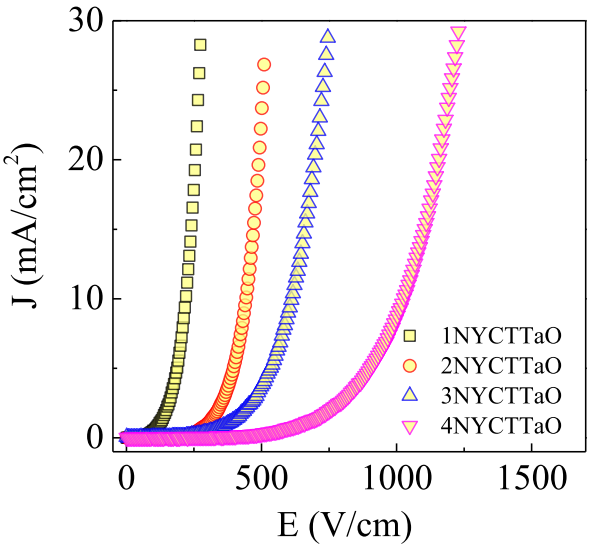

Fig. 11. J–E characteristics of $Na_{1/2}Y_{1/2}Cu_3Ti_{3.975}Ta_{0.025}O_{12}$ ceramics with different sintering durations and temperatures.

References

[1] Z.-M. Dang, J.-K. Yuan, J.-W. Zha, T. Zhou, S.-T. Li, G.-H. Hu, Fundamentals, processes and applications of high-permittivity polymer–matrix composites, Prog. Mater. Sci. 57 (2012) 660–723, https://doi.org/10.1016/j.pmatsci.2011.08.001.

[2] W. Wang, L. Li, T. Lu, R. Wang, N. Zhang, W. Luo, B. Zhang, Colossal permittivity in $BaTiO_3$-0.5wt%$Na_{0.5}Ba_{0.5}TiO_3$ ceramics with high insulation resistivity induced by reducing atmosphere, J. Eur. Ceram. Soc. 39 (2019) 4168–4176, https://doi.org/10.1016/j.jeurceramsoc.2019.06.006.

[3] X. Zhou, P. Liang, J. Zhu, Z. Peng, X. Chao, Z. Yang, Enhanced dielectric performance of $(Ag_{1/4}Nb_{3/4})_{0.01}Ti_{0.99}O_2$ ceramic prepared by a wet-chemistry method, Ceram. Int. 46 (2020) 11921–11925, https://doi.org/10.1016/j.ceramint.2020.01.229.

[4] J. Liu, C.-G. Duan, W.-G. Yin, W. Mei, R. Smith, J. Hardy, Large dielectric constant and Maxwell-Wagner relaxation in $Bi_{2/3}Cu_3Ti_4O_{12}$, Phys. Rev. B 70 (2004), 144106, https://doi.org/10.1103/PhysRevB.70.144106.

[5] T. Adams, D. Sinclair, A. West, Characterization of grain boundary impedances in fine- and coarse-grained $CaCu_3Ti_4O_{12}$ ceramics, Phys. Rev. B 73 (2006), 094124, https://doi.org/10.1103/PhysRevB.73.094124.

[6] M.A. Ramírez, P.R. Bueno, J.A. Varela, E. Longo, Non-Ohmic and dielectric properties of a $Ca_2Cu_2Ti_4O_{12}$ polycrystalline system, Appl. Phys. Lett. 89 (2006), 212102, https://doi.org/10.1063/1.2393122.

[7] P. Thongbai, T. Yamwong, S. Maensiri, V. Amornkitbamrung, P. Chindaprasirt, Improved dielectric and nonlinear electrical properties of fine-grained $CaCu_3Ti_4O_{12}$ ceramics prepared by a glycine-nitrate process, J. Am. Ceram. Soc. 97 (2014) 1785–1790, https://doi.org/10.1111/jace.12812.

[8] J. Boonlakhorn, N. Chanlek, P. Thongbai, P. Srepusharawoot, Strongly enhanced dielectric response and structural investigation of (Sr^{2+}, Ge^{4+}) Co-doped CCTO ceramics, J. Phys. Chem. C 124 (2020) 20682–20692, https://doi.org/10.1021/acs.jpcc.0c04484.

[9] S. Sharma, M.M. Singh, K.D. Mandal, Microstructure, crystal structure modelling and dielectric properties of $Y_{2/3}Cu_{3-x}Zn_xTi_4O_{12}$ (x = 0.10, 0.20 and 0.30) ceramics, New J. Chem. 42 (2018) 14655–14667, https://doi.org/10.1039/C8NJ02105H.

[10] Z. Tang, K. Wu, J. Li, S. Huang, Optimized dual-function varistor-capacitor ceramics of core-shell structured $xBi_{2/3}Cu_3Ti_4O_{12}/(1\text{-}x)CaCu_3Ti_4O_{12}$ composites, J. Eur. Ceram. Soc. 40 (2020) 3437–3444, https://doi.org/10.1016/j.jeurceramsoc.2020.03.034.

[11] T.B. Adams, D.C. Sinclair, A.R. West, Influence of processing conditions on the electrical properties of $CaCu_3Ti_4O_{12}$ ceramics, J. Am. Ceram. Soc. 89 (2006) 3129–3135, https://doi.org/10.1111/j.1551-2916.2006.01184.x.

[12] P. Liang, Y. Li, Y. Zhao, L. Wei, Z. Yang, Origin of giant permittivity and high-temperature dielectric anomaly behavior in $Na_{0.5}Y_{0.5}Cu_3Ti_4O_{12}$ ceramics, J. Appl. Phys. 113 (2013), 224102, https://doi.org/10.1063/1.4809927.

[13] L. Singh, B.C. Sin, I.W. Kim, K.D. Mandal, H. Chung, Y. Lee, J. Varela, A novel one-step flame synthesis method for tungsten-doped CCTO, J. Am. Ceram. Soc. 99 (2016) 27–34, https://doi.org/10.1111/jace.13930.

[14] L. Sun, R. Zhang, Z. Wang, E. Cao, Y. Zhang, L. Ju, Microstructure and enhanced dielectric response in Mg doped $CaCu_3Ti_4O_{12}$ ceramics, J. Alloys Compd. 663 (2016) 345–350, https://doi.org/10.1016/j.jallcom.2015.12.143.

[15] J. Boonlakhorn, N. Chanlek, J. Manyam, P. Srepusharawoot, S. Krongsuk, P. Thongbai, Enhanced giant dielectric properties and improved nonlinear electrical response in acceptor-donor (Al^{3+}, Ta^{5+})-substituted $CaCu_3Ti_4O_{12}$ ceramics, J. Adv. Ceram. 10 (2021) 1243–1255, https://doi.org/10.1007/s40145-021-0499-5.

[16] J. Boonlakhorn, P. Srepusharawoot, P. Thongbai, Distinct roles between complex defect clusters and insulating grain boundary on dielectric loss behaviors of (In^{3+}/Ta^{5+}) co-doped $CaCu_3Ti_4O_{12}$ ceramics, Results Phys. 16 (2020), 102886, https://doi.org/10.1016/j.rinp.2019.102886.

[17] L. Ni, M. Fu, Y. Zhang, Dielectric relaxation and relevant mechanism in giant dielectric constant $Sm_{2/3}Cu_3Ti_4O_{12}$ ceramics, J. Mater. Sci. Mater. Electron. 29 (2018) 17737–17742, https://doi.org/10.1007/s10854-018-9880-8.

[18] T.B.A. Derek, C. Sinclair, Finlay D. Morrison, Anthony R. West, $CaCu_3Ti_4O_{12}$: one-step internal barrier layer capacitor, Appl. Phys. Lett. 80 (12) (2002) 2153, https://doi.org/10.1063/1.1463211.

[19] P. Cheng, Z. Cao, M. Zhou, Q. Wang, S. Li, J. Li, Dielectric properties of $CaCu_3Ti_4O_{12}$ ceramics doped by La^{3+}, Ceram. Int. 45 (2019) 15320–15326, https://doi.org/10.1016/j.ceramint.2019.05.023.

[20] P. Thongbai, J. Jumpatam, T. Yamwong, S. Maensiri, Effects of Ta^{5+} doping on microstructure evolution, dielectric properties and electrical response in $CaCu_3Ti_4O_{12}$ ceramics, J. Eur. Ceram. Soc. 32 (2012) 2423–2430, https://doi.org/10.1016/j.jeurceramsoc.2012.02.048.

[21] P. Saengvong, N. Chanlek, P. Srepusharawoot, V. Harnchana, P. Thongbai, Enhancing giant dielectric properties of Ta^{5+}-doped $Na_{1/2}Y_{1/2}Cu_3Ti_4O_{12}$ ceramics by engineering grain and grain boundary, J. Am. Ceram. Soc. 105 (2022) 3447–3455, https://doi.org/10.1111/jace.18330.

[22] J. Boonlakhorn, J. Manyam, P. Srepusharawoot, S. Krongsuk, P. Thongbai, Effects of charge compensation on colossal permittivity and electrical properties of grain boundary of $CaCu_3Ti_4O_{12}$ ceramics substituted by Al^{3+} and Ta^{5+}/Nb^{5+}, Molecules 26 (2021) 3297, https://doi.org/10.3390/molecules26113294.

[23] S.-Y. Chung, J.-H. Choi, J.-K. Choi, Tunable current-voltage characteristics in polycrystalline calcium copper titanate, Appl. Phys. Lett. 91 (2007), 091912, https://doi.org/10.1063/1.2777184.

[24] R. Schmidt, M.C. Stennett, N.C. Hyatt, J. Pokorny, J. Prado-Gonjal, M. Li, D.C. Sinclair, Effects of sintering temperature on the internal barrier layer capacitor (IBLC) structure in $CaCu_3Ti_4O_{12}$ (CCTO) ceramics, J. Eur. Ceram. Soc. 32 (2012) 3313–3323, https://doi.org/10.1016/j.jeurceramsoc.2012.03.040.

[25] P. Thongbai, B. Putasaeng, T. Yamwong, S. Maensiri, Current–voltage nonlinear and dielectric properties of $CaCu_3Ti_4O_{12}$ ceramics prepared by a simple thermal decomposition method, J. Mater. Sci. Mater. Electron. 23 (2012) 795–801, https://doi.org/10.1007/s10854-011-0494-7.

[26] P. Liang, Y. Li, F. Li, X. Chao, Z. Yang, Effect of the synthesis route on the phase formation behavior and electric property of $Na_{0.5}Bi_{0.5}Cu_3Ti_4O_{12}$ ceramics, Mater. Res. Bull. 52 (2014) 42–49, https://doi.org/10.1016/j.materresbull.2014.01.009.

[27] P. Liu, Y. Lai, Y. Zeng, S. Wu, Z. Huang, J. Han, Influence of sintering conditions on microstructure and electrical properties of $CaCu_3Ti_4O_{12}$ (CCTO) ceramics, J. Alloys Compd. 650 (2015) 59–64, https://doi.org/10.1016/j.jallcom.2015.07.247.

[28] Z. Liu, Z. Yang, High permittivity, low dielectric loss and impedance characteristics of $Li_{0.5}La_{0.5}Cu_3Ti_4O_{12}$ ceramics by a sol–gel technique, J. Electron. Mater. 48 (2019) 5333–5341, https://doi.org/10.1007/s11664-019-07344-x.

[29] A.K. Thomas, M. George, D. Sajan, K. Abraham, J. Thomas, K.V. Saban, Effect of niobium doping on the dielectric and nonlinear current–voltage characteristics of $Na_{0.5}La_{0.5}Cu_3Ti_4O_{12}$ ceramics, Opt. Mater. 89 (2019) 299–307, https://doi.org/10.1016/j.optmat.2019.01.045.

[30] X. Wang, P. Liang, Z. Peng, H. Peng, Y. Xiang, X. Chao, Z. Yang, Significantly enhanced breakdown electric field in Zn-doped $Y_{2/3}Cu_3Ti_4O_{12}$ ceramics, J. Alloys Compd. 778 (2019) 391–397, https://doi.org/10.1016/j.jallcom.2018.11.104.

[31] Z. Peng, X. Zhou, J. Wang, J. Zhu, P. Liang, X. Chao, Z. Yang, Origin of colossal permittivity and low dielectric loss in $Na_{1/3}Cd_{1/3}Y_{1/3}Cu_3Ti_4O_{12}$ ceramics, Ceram. Int. 46 (2020) 11154–11159, https://doi.org/10.1016/j.ceramint.2020.01.136.

[32] M.M. Ahmad, H.M. Kotb, C. Joseph, S. Kumar, A. Alshoaibi, Transport and dielectric properties of mechanosynthesized $La_{2/3}Cu_3Ti_4O_{12}$ ceramics, Crystals 11 (2021) 313, https://doi.org/10.3390/cryst11030313.

[33] J. Deng, L. Liu, X. Sun, S. Liu, T. Yan, L. Fang, B. Elouadi, Dielectric relaxation behavior and mechanism of $Y_{2/3}Cu_3Ti_4O_{12}$ ceramic, Mater. Res. Bull. 88 (2017) 320–329, https://doi.org/10.1016/j.materresbull.2017.01.005.

[34] S. Sharma, M.M. Singh, K.D. Mandal, Microstructure and magnetic properties of $Y_{2/3}Cu_3Ti_4O_{12}$ ceramic, New J. Chem. 41 (2017) 10383–10389, https://doi.org/10.1039/C7NJ02122D.

[35] J. Jumpatam, A. Mooltang, B. Putasaeng, P. Kidkhunthod, N. Chanlek, P. Thongbai, S. Maensiri, Effects of Mg^{2+} doping ions on giant dielectric properties and electrical responses of $Na_{1/2}Y_{1/2}Cu_3Ti_4O_{12}$ ceramics, Ceram. Int. 42 (2016) 16287–16295, https://doi.org/10.1016/j.ceramint.2016.07.167.

[36] W. Somphan, N. Sangwong, T. Yamwong, P. Thongbai, Giant dielectric and electrical properties of sodium yttrium copper titanate: $Na_{1/2}Y_{1/2}Cu_3Ti_4O_{12}$, J. Mater. Sci. Mater. Electron. 23 (2012) 1229–1234, https://doi.org/10.1007/s10854-011-0578-4.

[37] J. Jumpatam, W. Somphan, J. Boonlakhorn, B. Putasaeng, P. Kidkhunthod, P. Thongbai, S. Maensiri, Non-ohmic properties and electrical responses of grains and grain boundaries of $Na_{1/2}Y_{1/2}Cu_3Ti_4O_{12}$ ceramics, J. Am. Ceram. Soc. 100 (2017) 157–166, https://doi.org/10.1111/jace.14473.

[38] P. Saengvong, N. Chanlek, P. Srepusharawoot, V. Harnchana, P. Thongbai, Enhancing giant dielectric properties of Ta^{5+}-doped $Na_{1/2}Y_{1/2}Cu_3Ti_4O_{12}$ ceramics by engineering grain and grain boundary, J. Am. Ceram. Soc. 105 (2022) 3447–3455, https://doi.org/10.1111/jace.18330.

[39] G. Kresse, J. Furthmüller, Efficiency of ab-initio total energy calculations for metals and semiconductors using a plane-wave basis set, Comput. Mater. Sci. 6 (1996) 15–50, https://doi.org/10.1016/0927-0256(96)00008-0.

[40] J.P. Perdew, K. Burke, M. Ernzerhof, Generalized gradient approximation made simple, Phys. Rev. Lett. 77 (1996) 3865–3868, https://doi.org/10.1103/PhysRevLett.77.3865.

[41] P. Saengvong, N. Chanlek, B. Putasaeng, A. Pengpad, V. Harnchana, S. Krongsuk, P. Srepusharawoot, P. Thongbai, Significantly improved colossal dielectric properties and maxwell-wagner relaxation of TiO_2-rich $Na_{1/2}Y_{1/2}Cu_3Ti_{4+x}O_{12}$ ceramics, Molecules 26 (2021), https://doi.org/10.3390/molecules26196043.

[42] H. Man, W. Ye, L. Zhang, Y. Deng, S. Zhong, S. Du, D. Xu, Effects of Y Doping on dielectric and varistor properties of $CaCu_3Ti_4O_{12}$ thin films, J. Electron. Mater. 49 (2020) 7379–7385, https://doi.org/10.1007/s11664-020-08515-x.

[43] F. Han, S. Ren, J. Deng, T. Yan, X. Ma, B. Peng, L. Liu, Dielectric response mechanism and suppressing high-frequency dielectric loss in Y_2O_3 grafted $CaCu_3Ti_4O_{12}$ ceramics, J. Mater. Sci. Mater. Electron. 28 (2017) 17378–17387, https://doi.org/10.1007/s10854-017-7671-2.

[44] R.D. Shannon, Revised effective ionic radii and systematic studies of interatomic distances in halides and chalcogenides, Acta Crystallogr. A 32 (1976) 751–767, https://doi.org/10.1107/s0567739476001551.

[45] J. Boonlakhorn, P. Suksangrat, N. Chanlek, W. Sarakorn, S. Krongsuk, P. Thongbai, P. Srepusharawoot, Dielectric properties with high dielectric permittivity and low loss tangent and nonlinear electrical response of sol-gel synthesized $Na_{1/2}Sm_{1/2}Cu_3Ti_4O_{12}$ perovskite ceramic, J. Eur. Ceram. Soc. 42 (2022) 5659–5668, https://doi.org/10.1016/j.jeurceramsoc.2022.06.030.

[46] J. Boonlakhorn, N. Chanlek, P. Suksangrat, P. Thongbai, P. Srepusharawoot, Colossal dielectric properties of $Na_{1/3}Ca_{1/3}Sm_{1/3}Cu_3Ti_4O_{12}$ ceramics: computational and experimental investigations, Ceram. Int. (2022), https://doi.org/10.1016/j.ceramint.2022.09.131.

[47] J. Jumpatam, W. Somphan, B. Putasaeng, N. Chanlek, P. Kidkhunthod, P. Thongbai, S. Maensiri, Nonlinear electrical properties and giant dielectric response in $Na_{1/3}Ca_{1/3}Y_{1/3}Cu_3Ti_4O_{12}$ ceramic, Mater. Res. Bull. 90 (2017) 8–14, https://doi.org/10.1016/j.materresbull.2017.02.014.

[48] S.-Y. Lee, H.E. Kim, S.-I. Yoo, Subsolidus phase relationship in the CaO–CuO–TiO_2 ternary system at 950°C in air, J. Am. Ceram. Soc. 97 (2014) 2416–2419, https://doi.org/10.1111/jace.13119.

[49] K.M.A. Salam, H. Fukuda, S. Nomura, Effects of additive elements on improvement of the dielectric properties of Ta_2O_5films formed by metalorganic decomposition, J. Appl. Phys. 93 (2003) 1169–1175, https://doi.org/10.1063/1.1532940.

[50] L. Bai, Y. Wu, L. Zhang, Influence of FeNb codoping on the dielectric and electrical properties of $CaCu_3Ti_4O_{12}$ ceramics, J. Alloys Compd. 661 (2016) 6–13, https://doi.org/10.1016/j.jallcom.2015.11.142.

[51] L. Ni, X.M. Chen, Enhancement of giant dielectric response in $CaCu_3Ti_4O_{12}$ ceramics by Zn substitution, J. Am. Ceram. Soc. 93 (2010) 184–189, https://doi.org/10.1111/j.1551-2916.2009.03384.x.

[52] J. Boonlakhorn, P. Kidkhunthod, P. Thongbai, A novel approach to achieve high dielectric permittivity and low loss tangent in $CaCu_3Ti_4O_{12}$ ceramics by co-doping with Sm^{3+} and Mg^{2+} ions, J. Eur. Ceram. Soc. 35 (2015) 3521–3528, https://doi.org/10.1016/j.jeurceramsoc.2015.06.008.

[53] J. Zhao, M. Chen, Q. Tan, Embedding nanostructure and colossal permittivity of TiO_2-covered CCTO perovskite materials by a hydrothermal route, J. Alloys Compd. 885 (2021), 160948, https://doi.org/10.1016/j.jallcom.2021.160948.

[54] J. Boonlakhorn, P. Kidkhunthod, B. Putasaeng, P. Thongbai, Significantly improved non-Ohmic and giant dielectric properties of $CaCu_{3-x}Zn_xTi_4O_{12}$ ceramics by enhancing grain boundary response, Ceram. Int. 43 (2017) 2705–2711, https://doi.org/10.1016/j.ceramint.2016.11.089.

[55] D.P. Samarakoon, N. Govindaraju, R.N. Singh, Influence of atmospheres on the dielectric properties of calcium copper titanate ceramics, J. Am. Ceram. Soc. 102 (2019) 5271–5283, https://doi.org/10.1111/jace.16381.

[56] J. Zhao, H. Zhao, Z. Zhu, Influence of sintering conditions and CuO loss on dielectric properties of $CaCu_3Ti_4O_{12}$ ceramics, Mater. Res. Bull. 113 (2019) 97–101, https://doi.org/10.1016/j.materresbull.2019.01.014.

[57] S.-Y. Chung, I.-D. Kim, S.-J.L. Kang, Strong nonlinear current–voltage behaviour in perovskite-derivative calcium copper titanate, Nat. Mater. 3 (2004) 774–778, https://doi.org/10.1038/nmat1238.

[58] Y.-H. Lin, J. Cai, M. Li, C.-W. Nan, J. He, Grain boundary behavior in varistor-capacitor TiO_2-rich $CaCu_3Ti_4O_{12}$ ceramics, J. Appl. Phys. 103 (2008), 074111, https://doi.org/10.1063/1.2902402.